Direct Observation of Li-Ion Transport in Electrodes under Nonequilibrium Conditions Using Neutron Depth Profiling

*Xiaoyu Zhang, Tomas W. Verhallen, Freek Labohm, and Marnix Wagemaker**

One of the key challenges of Li-ion electrodes is enhancement of (dis)charge rates. This is severely hindered by the absence of a technique that allows direct and nondestructive observation of lithium ions in operating batteries. Direct observation of the Li-ion concentration profiles using operando neutron depth profiling reveals that the rate-limiting step is depended not only on the electrode morphology but also on the cycling rate itself. In the $LiFePO_4$ electrodes phase nucleation limits the charge transport at the lowest cycling rates, whereas electronic conductivity is rate limiting at intermediate rates, and only at the highest rates ionic transport through the electrode is rate limiting. These novel insights into electrode kinetics are imperative for the improvement of Li-ion batteries and show the large value of in situ NDP in Li-ion battery research and development.

1. Introduction

Development of high-energy density Li-ion batteries is essential for the realization of electric and plug-in hybrid vehicles. Aiming at performance improvement, considerable efforts are made to understand the fundamental mechanisms that limit the (dis)charge rates of Li-ion battery materials.[1,2] During charge Li-ions are driven from the positive electrode to the anode by an externally applied potential. The larger lithium chemical potential in the negative electrode is the driving force for the exothermic discharge reaction due to which the Li-ions migrate back to the positive electrode. The internal resistance of the battery results in a voltage polarization, or overpotential, that scales with the (dis)charge current, leading to higher external potentials during charge and lower during discharge, reducing the energy efficiency of the battery. Because the internal resistance of the battery is dominated by the resistance of the rate-limiting step, higher power densities, and hence shorter (dis)charge times, require improvement of the rate-limiting charge transport step. Therefore, knowledge of what charge transport phenomenon is rate limiting under what conditions is paramount for the design of future Li-ion batteries.

Possible contributions to the internal resistance include (1) the electronic wiring (the contact between the active electrode material and current collector), (2) the ionic network formed by the liquid electrolyte in the pores of the composite electrodes connecting the active electrode material and the electrolyte, (3) the charge transfer reaction between the liquid electrolyte and the active electrode material, and (4) the solid state transport and phase nucleation/transformation kinetics within the active electrode material.

Many processes have been reported to improve Li-ion battery (dis)charge kinetics each improving one or more of the described aspects 1–4 illustrating the complexity and the lack of agreement concerning the rate-limiting step. This is best illustrated by $LiFePO_4$, an important electrode material proposed by Padhi et al.[3] in 1997, and an intensively studied, well-established model system up to date. (a) For $LiFePO_4$ the initial hurdle of poor intrinsic electronic and solid-state ionic conduction were overcome by reducing the particle size in combination with carbon or metallic conducting coatings.[4–6] In addition to the trivial decrease in the solid-state diffusion distance, particle size reduction toward the nano range has also shown to impact the kinetic and thermodynamic properties of electrode materials.[7–10] For instance, the nucleation barrier for the first-order phase transition in $LiFePO_4$ is predicted to be smaller for smaller particles.[11] Also, the equilibrium potential depends on the particle size, which is predicted to be the consequence of the surface energy which has more impact in smaller particles.[7,12–14] In $LiFePO_4$ this results in a larger equilibrium voltage in smaller $LiFePO_4$ particles[12,15] which explains the spontaneous, without an externally applied potential, Li-ion transport from small to large $LiFePO_4$ particles.[16] (b) First-order phase transitions are generally thought to result in poor kinetics as compared to solid solution reactions. The observation that the first-order phase transition can be bypassed in $LiFePO_4$ at high (dis)charge rates[17,18] driven by the overpotential,[19–21] is also considered to be responsible for the high (dis)charge rates that can be achieved.[17–21] (c) Surface diffusion on the $LiFePO_4$ particles appears to play a role as very fast (dis)charge rates were achieved by the addition of an ionic-conducting phase at the $LiFePO_4$ surface.[22] (d) In many studies it has been recognized that for higher rates the ionic transport through the porous electrode structure is rate limiting.[23–29] This is consistent with the direct observation that the electrode capacity decreases with increasing thickness at the same rate and loading density.[23,30] Over the years, various modelling approaches have been describing the complex phenomena that play a role, mainly focussing on the with the ion transport and charge transfer through the porous electrode matrix,[1,31] solid solutions and distributed ohmic drop in the

X. Zhang, T. W. Verhallen, F. Labohm, Dr. M. Wagemaker
Department of Radiation Science and Technology
Delft University of Technology
Mekelweg 15, 2629JB Delft, The Netherlands
E-mail: m.wagemaker@tudelft.nl

DOI: 10.1002/aenm.201500498

$LiFePO_4$ material,[32] and the complex phase behavior in the solid-state $LiFePO_4$[11,33,34] material. The diverse results, caused by the large amount of parameters involved, have to date made it impossible to unambiguously determine the rate-limiting charge transport mechanism under various conditions, which is crucial for improving battery performance.

Depending on which charge transport mechanism is rate limiting distinctly different Li-ion distributions are expected throughout the electrodes perpendicular to the current collector. Therefore, direct observation of the Li-ion distribution depending on the electrochemical conditions and depending on the structure and morphology of the electrodes would give direct mechanistic insights into kinetic and thermodynamic processes in batteries, currently only partially available. For this reason, experimental methods are required that probe the distribution of Li-ions directly under nondestructive in operando conditions. This has driven the development of in situ techniques such as transmission electron microscopy (TEM),[35] in situ nuclear magnetic resonance (NMR),[36,37] neutron imaging,[38–40] and neutron depth profiling (NDP).[41–46]

NDP offers the possibility of directly seeing lithium nuclei through the capture reaction of neutrons with the ^6Li isotope to form an α-particle (^4He) and a triton (^3H) according to

$$^6Li + n_{th} \rightarrow {}^4He(2055keV) + {}^3H(2727keV)$$

The energy that is generated by the reaction is distributed between the two particles according to conservation of energy and momentum. The ^4He and ^3H particles travel through the surrounding material during which they lose energy. By measuring this energy loss the depth at which the ^6Li atom was located can be determined. This allows reconstructing a Li-atom density profile as a function of depth, shown in **Figure 1**, without significantly influencing the Li concentration due to the low neutron flux making this a nondestructive technique.

The history of the using of neutron caption reactions can be traced back to 1972. Ziegler et al. first used this reaction to determine the concentration of boron impurities in silicon wafers.[47] After that, Downing et al.[48] and Biersack et al.[49] used this method to measure other isotopes, including ^6Li. This initiated Whitney et al.[50] and Nagoure et al.[51–53] to use NDP to measure postmortem lithium concentration profiles in the near surface area of commercial Li-ion batteries resulting in more insight into battery degradation after many charge/discharge cycles. Oudenhoven et al.[54] performed the first in situ NDP study on thin film solid-state microbatteries, demonstrating the direct observation of the evolution of the lithium concentration profile over time under different electrochemical conditions. The challenge of applying in situ NDP to conventional Li-ion batteries is the limited travel length of the charged capture reaction products through the electrode and current collector, limiting the maximum depth in the battery that can be probed. An additional complication is that NDP experiments are typically performed under vacuum conditions, preventing parasitic energy absorption of the capture reaction products in air. As a consequence of the low outside pressure, the electrolyte tends to become gaseous, compromising the contact between the electrodes and the separator. Recently, Wang et al.[41] and Liu et al.[46] reported on the development of in situ NDP elegantly

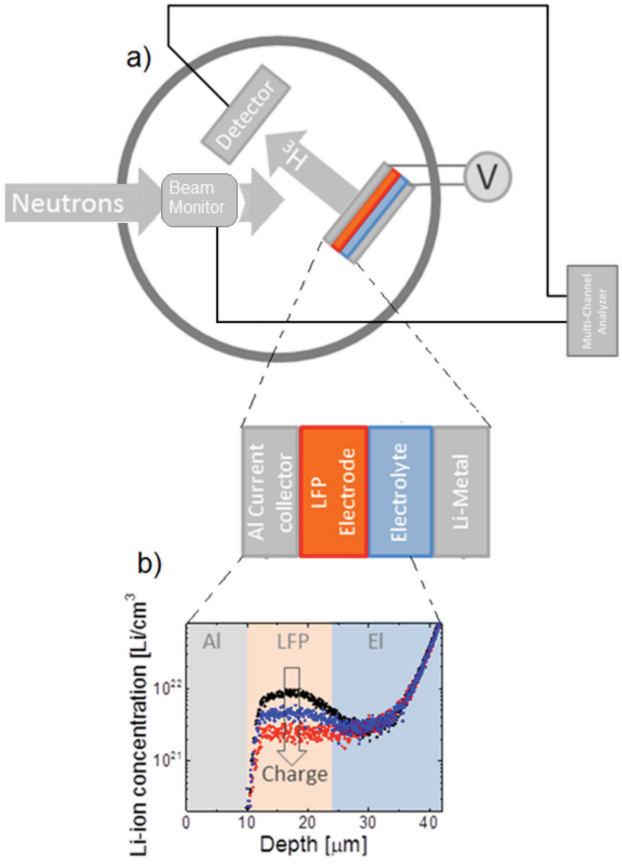

Figure 1. a) The schematic NDP setup at the Reactor Institute Delft. b) Depth-calibrated lithium intensity plot indicating the layered battery geometry.

demonstrating the onset of lithiation in Sn electrodes and giving mechanistic insight into the process. Employing half-cells, with Kapton film windows to protect the lithiated surface of the Sn sample, Wang et al. were able to determine the Li distribution inside the Sn quantitatively down to several micrometers and thereby enabled studying these liquid electrolyte systems with in situ NDP. The further developed cell design by Liu et al. allowed clear observation of the Li distribution during charge and discharge of a lithium–tin cell, proving operando NDP as an invaluable technique for the characterization of Li-ion battery electrode materials. Recently, we reported on extending the application of in situ NDP toward conventional Li-ion battery systems, using the Al current collector as window, allowing probing relatively thick electrodes with liquid electrolytes.[43–45] This is another significant step forward because the developed cell allows any type of electrode coating to be analyzed with in situ NDP.

The present communication aims at direct insight into the processes that limit the charge transport in Li-ion batteries by measuring the lithium distribution in porous $LiFePO_4$ electrodes, in combination with liquid electrolytes, using operando NDP under dynamic charge/discharge conditions. By varying the electrode morphology, including the electronic wiring and particle size, it is shown what process is rate limiting under what conditions, providing fundamental understanding and

guidance to the development of high-performance Li-ion battery electrodes.

2. Results and Discussion

Figure 1 shows the schematic setup of the operando NDP experiments. The designed NDP cell is exposed to the thermal neutron beam at the $LiFePO_4$ electrode side inside the vacuum chamber. The capture reaction of the incoming thermal neutrons with the ^{6}Li-ions forms an α-particle (^{4}He) and a triton (^{3}H) with 2055 and 2727 keV, respectively. Because of the larger ^{4}He stopping power in the electrode and current collector and the lower initial kinetic energy, ^{4}He particles are not able to penetrate through the current collector, and are consequently not detected. As a consequence, the results in this communication are based on ^{3}H spectra.

The depth calibrated spectra in Figure 1b demonstrate that the thickness of the aluminum current collector is approximately 10 µm and that this specific $LiFePO_4$ electrode is approximately 12 µm thick. This is relatively thin for Li-ion electrodes, but it has the advantage for the NDP experiments that complete electrode is probed. The kinetic energy of the ^{3}H particles limits the escape depth through the layered battery geometry to roughly 40 µm. Consequently, ^{3}H originating from the Li-metal negative electrode and large part of the electrolyte/separator are not able to reach the detector. The calibrated Li density measured with NDP indicates that these electrodes are homogeneous, with a density (2 g cm^{-3}) consistent with that measured via the electrode loading and thickness, see the Supporting Information. The lithium concentration in the $LiFePO_4$ active material (13.8×10^{21} Li cm^{-3} or 22.8 molar) is much larger compared to that in the electrolyte (0.6×10^{21} Li cm^{-3} or 1.0 molar) in the pores of the positive electrode. For the present electrode-coating density, 2.0 g cm^{-3} (34% porous), almost 98% of the signal is due to lithium in the active $LiFePO_4$ material. Therefore, the Li-ion depth profiles in this work are only due to the Li ions in the active material, and hence the measured Li concentration can be expressed in the average local Li composition in the active material. Note that all Li-ion depth profiles will be consistently plotted with the interface between the aluminum current collector and the $LiFePO_4$ electrode at the left side (zero depth) and the interface between the $LiFePO_4$ electrode and the electrolyte at the right side.

The in situ evolution of the Li-ion concentration as a function of depth and time in the $LiFePO_4$ electrode (140 ± 56 nm particle size, see the Supporting Information, Figure S5) during a full C/50 charge–discharge cycle is shown in **Figure 2**b. The ^{3}H counts were converted to Li-ion concentration by subtracting the fully (C/50) charged state spectrum ($Li_{x=0}FePO_4$) from all the spectra to eliminate the background and by normalizing on the fully discharged state ($Li_{x=1}FePO_4$). This facilitates comparing concentrations at different depths as is illustrated in Figure 2a. As a cross-check the count rate was also corrected for the experimental geometry using a calibration sample and the stopping power of the current collector and electrode resulting in the same maximum average Li occupancy taking into account the electrode density, see the Supporting Information.

The operando evolution of the Li-ion distribution in the $LiFePO_4$ electrode during a C/50 charge–discharge cycle is shown in Figure 2b. As expected during charging the Li-ion concentration decreases throughout the electrode and during discharge the Li-ion concentration increases again, illustrating the reversible reaction of all the Li ions in $LiFePO_4$. Figure 2a displays no significant difference between charge and discharge Li-ion concentration profiles proving the Li-ion depletion and insertion to be homogeneous during both slow charge and discharge. Using phase field modeling in combination with porous diffusion theory, Ferguson et al.[34] predicted a sharp gradient in the Li-ion distribution in the electrode material at low rates (C/30) assuming no particle size distribution, whereas a homogeneous distribution in the Li-ion concentration was predicted

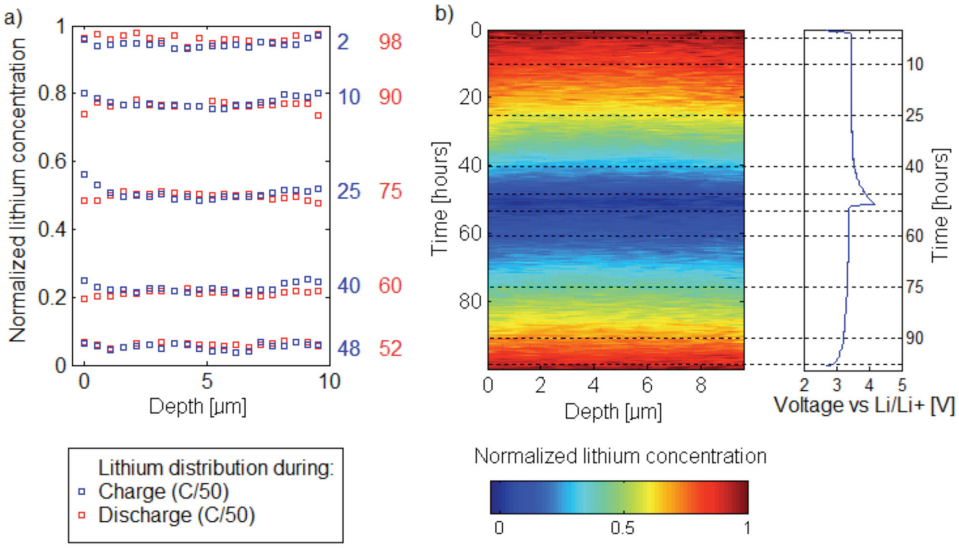

Figure 2. a) Comparing the charged and discharged states at several stages during a complete C/50 charge discharge cycle. b) Evolution of the lithium concentration during charge and discharge at C/50. The dotted lines indicate the states compared in (a). The current collector is located at the left and the electrolyte at the right.

when a distribution of particle sizes was introduced,[55] in agreement with the slow cycling result in Figure 2 for 140 ± 56 nm particles.

To study the impact of particle size on the distribution of Li ions in electrodes in detail, two double-layered electrode geometries have been prepared, geometry 1 consisting of an approximately 5 mm thick layer of 70 ± 11 nm $LiFePO_4$ particles (see the Supporting Information, Figure S5) at the current collector side and an approximately 5 µm thick layer of 140 ± 56 nm particles at the electrolyte side and geometry 2 vice versa. Particle size is known to influence the equilibrium potential[12,56] being larger in smaller $LiFePO_4$ crystallites[12,15,16] and in addition it has been predicted to influence the nucleation barrier being lower in smaller $LiFePO_4$ crystallites due to surface wetting.[11] As a consequence, two different situations may occur depending on the timescale of the (dis)charge experiment. (1) Given enough time the Li-ion extraction and insertion may be expected to follow the thermodynamic route in which case larger particles (140 nm) will be depleted from Li ions first during charge (their lower equilibrium Li-ion storage potential will lead to preferential nucleation of the $FePO_4$ phase) and inserted first during discharge. (2) In contrast, if the nucleation kinetics are dominant in comparison to the other kinetic processes (charge transfer and ionic and electronic conduction) the $FePO_4$ phase will nucleate first in smaller particles (70 nm) based on their lower predicted nucleation energies.[11]

The in situ NDP during C/10 charging in **Figure 3** shows that independent of the geometry the smaller (70 nm) particles delithiate first. Apparently, the nonequilibrium pathway is followed during charge indicating that the nucleation energy for the phase transition in the smaller $LiFePO_4$ particles is lower compared to that in the larger particles, providing the first direct experimental evidence for the prediction by Cogswell et al.[11] Figure 3 shows that also during discharge the smaller particles react first. In this case, however, the thermodynamic route (based on the difference in Li-ion potential) and the kinetic route (based on the difference in nucleation energy) coincide, but given that on charge the lower nucleation energy of smaller particles appears to be dominant, it is likely this is also the case during discharge. The fact that particle size determines the Li-ion distribution in electrodes implies that both electronic and ionic conduction through the electrode do not play a dominant role (are not mainly responsible for the observed Li-ion gradient) up to C/10 in these electrode morphologies. Note that the preferential reaction of the smaller particles is the origin of the absence of a Li-ion gradient at low rates for homogeneous electrodes having a particle size distribution as shown in Figure 2 and predicted recently.[55]

To investigate what charge transport mechanisms play a role at C/10 and beyond experiments were performed on homogeneous electrodes using an average $LiFePO_4$ particle size of 140 ± 56 nm. Contrary to what was observed at C/50 the concentration profiles at C/10 shown in **Figure 4** reveal a small, but well-resolved, Li-ion gradient. Comparing the charge and discharge states in Figure 4a shows that part of the electrode located near the current collector appears to be more reactive. During charge Li ions deplete first near the current collector side and during discharge Li ions are first inserted near the current collector side. This Li-ion gradient throughout the electrode provides insight into which charge transport process limits the (dis)charge rate in these electrodes. If charge transfer over the electrolyte-active material interface (located in the pores of the electrode) or the phase nucleation/transition kinetics in the active material would be rate limiting, no Li-ion gradient should be expected over the depth of the electrode, as was observed at lower rates.

However, because part of the electrode near current collector is more reactive, the electronic conductivity throughout the electrode must be the origin of the observed Li-ion gradient at C/10. Apparently, the electronic wiring provided by the 10% carbon black in combination with the carbon coating of the $LiFePO_4$ particles dominates the internal resistance of the battery at this rate. To investigate this intriguing finding the same C/10 charge discharge experiment was repeated with a $LiFePO_4$ electrode having a much larger (50%) carbon black content with the intention to improve the electronic wiring throughout the electrode. The result is shown in Figure 4b where the signal-to-noise ratio is compromised due to the decrease in active material reducing the amount of lithium present which decreases the detected ^3H intensity. The small difference between charge and discharge and the absence of a clear gradient indicate that the increase in carbon black content improved the electronic conductivity of the electrode lifting the Li-ion gradient observed in Figure 4a. Generally, Li-ion diffusion limitations through the electrode/electrolyte matrix are predicted to limit overall charge transport[57,58,63] and electronic resistance is not considered. The present results show that even for carbon-coated $LiFePO_4$ in combination with 10 wt% carbon black electronic conduction can dominate charge transport through porous electrodes, indicating this is an important factor to be considered in kinetic modeling of electrodes.

The time resolution of in situ NDP setup is limited by the neutron flux, which in the present setup is approximately 5 min, thus limiting operando NDP to approximately 1 C cycling rates. Therefore, concentration gradients at higher rates were measured under ex situ conditions. To minimize relaxation effects due to ionic and electronic exchange between the particles within the electrode, batteries were disassembled and the electrode washed with DMC (dimethyl carbonate) within 2 min after charging to the desired state.

The normalized Li-ion concentration after a 30 min charge at 1 C rate is shown in **Figure 5**a. The preferential Li-ion depletion at the current collector side (left side of the Li-ion concentration profiles), resulting in approximately 30% difference in concentration compared to the electrolyte side, indicates that even at 1 C the electronic conduction throughout the porous electrode matrix limits the overall charge transfer. However increasing the charge rate to 5 C, shown in Figure 5b, and to 20 C, shown in Figure 5c, completely changes this picture. At 5 C no Li-ion gradient is observed and at 20 C the gradient inverses, indicating that Li-ion depletion predominantly takes place at the electrolyte side (right side of the Li-ion concentration profiles). This indicates that at high rate (20 C) conditions the gradient is caused by Li-ion transport limitations throughout the electrode matrix. We anticipate that in this case the ionic wiring, the Li-ion transport through the electrolyte in the pores of the electrode, dominates the internal resistance of the battery. Although direct observation of Li-ion gradients has been unavailable up to date, it has been long recognized that in many cases the ionic transport through the electrolyte

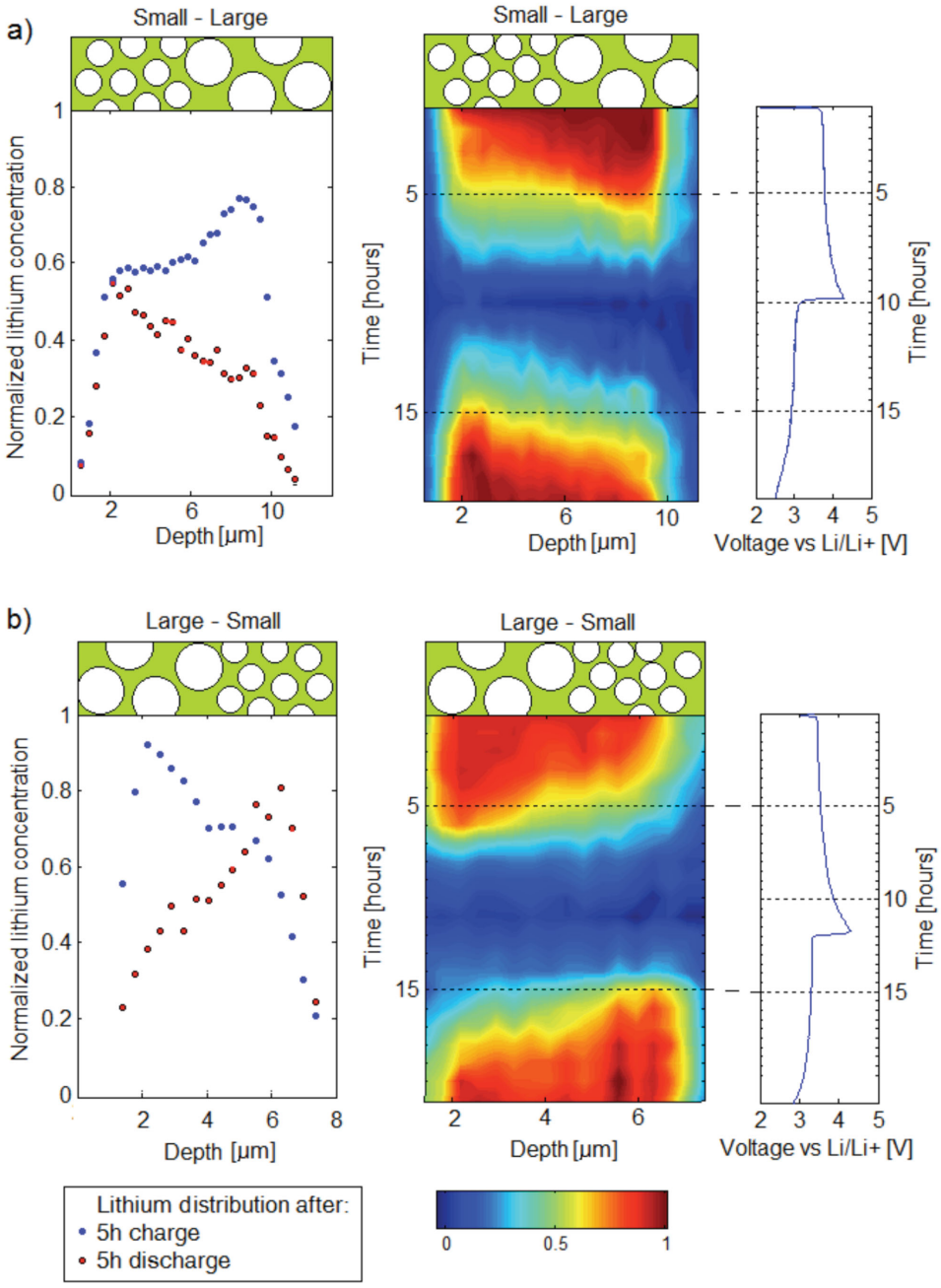

Figure 3. In situ NDP spectra during C/10 cycling: a) geometry 1; small (70 nm) particles at the current collector side and large (140 nm) particles at the electrolyte side. Left: Li-ion distribution after 5 h of charge and discharge. Right: evolution of the Li-ion distribution during a full charge discharge cycle. b) Geometry 2; large (140 nm) particles at the current collector side and small (70 nm) particles at the electrolyte side. Left: Li-ion distribution after 5 h of charge and discharge. Right: evolution of the Li-ion distribution during a full charge discharge cycle. The current collector is located at the left and the electrolyte at the right.

and through the porous electrode structure is rate limiting and not the electrode material itself.[23–30,58] This is also supported by the decreasing capacity at the same (dis)charge rate, while increasing the electrode thickness.[23,59] Interestingly, at 5 C electronic conduction and ionic conduction appear to become comparable, which cancels out the gradient. Thereby, Figure 5 demonstrates the transition in rate-limiting charge transport process from electronic conduction up to 1 C, which is canceled out at 5 C by ionic transport limitations, the latter dominating above 5 C.

It should be realized that the rates at which the transition between the different rate-limiting charge transport mechanisms takes place strongly depends on the electrode morphology (i.e., thickness, porosity, and tortuosity) formulation (i.e., weight percentage active material, conductive additive, etc.), electrolyte (molarity and conductivity), and the electrode material

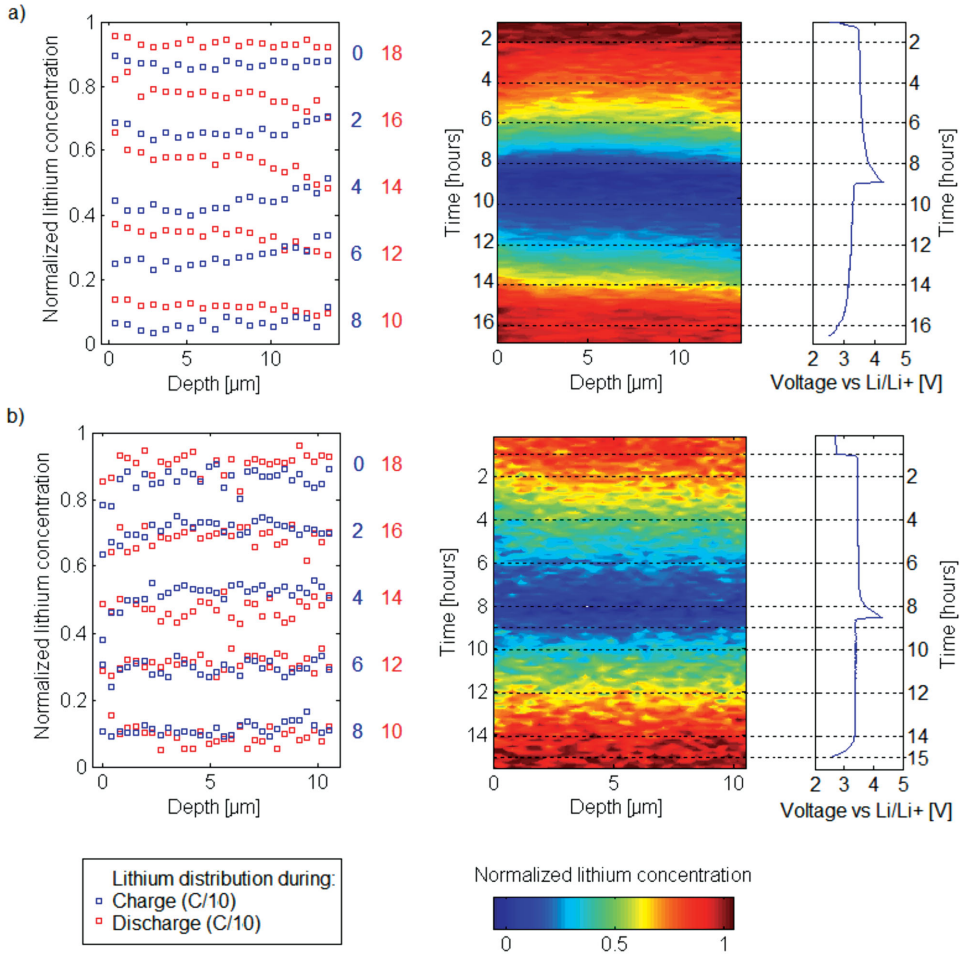

Figure 4. Lithium distribution in $LiFePO_4$ (140 nm) electrodes cycled at C/10. a) With 10% carbon black as conductive additive and b) with 50% carbon black as conductive additive. Left: Li-ion concentrations at various stages during charge and discharge where the label at the right axis indicates the time in hours in the voltage profile, right: concentration evolution during a full cycle including the voltage profile. The current collector is located at the left and the electrolyte at the right.

properties itself. Typically, the ionic and electronic conductivity strongly depend on the porosity of the electrode matrix having an optimum around 35% porosity[25] which is typically aimed for in electrode preparation. Given the current results it is interesting to find how nucleation, electronic, and ionic conduction play a role at variable cycling rates in other two phase materials. Another challenge is to find out how the observed asymmetry between charge and discharge[60] influences the Li-ion gradients and rate-limiting transport mechanisms, subject of our future studies.

Figure 6 shows a double logarithmic plot of the overpotential versus the charge rate during galvanostatic experiments where the overpotential was selected at the onset of the voltage plateau. Three different charge rate regions can be distinguished that can be correlated to the different rate-limiting charge transport mechanisms observed directly in the Li-ion concentration profiles using NDP. At low rates, C/50–C/10, the particle size depended two-phase nucleation dominates the charge transport, demonstrated in Figure 3 where the smaller $LiFePO_4$ particles show to have

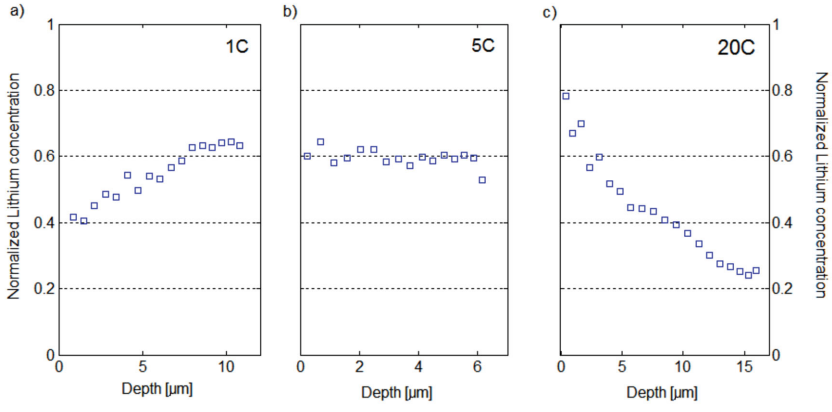

Figure 5. Normalized Li-ion concentrations measured ex situ, a) after 30 min charge at 1 C, b) after 6 min charge at 5 C, and c) after 2 min charge at 20 C. The current collector is located at the left and the electrolyte at the right.

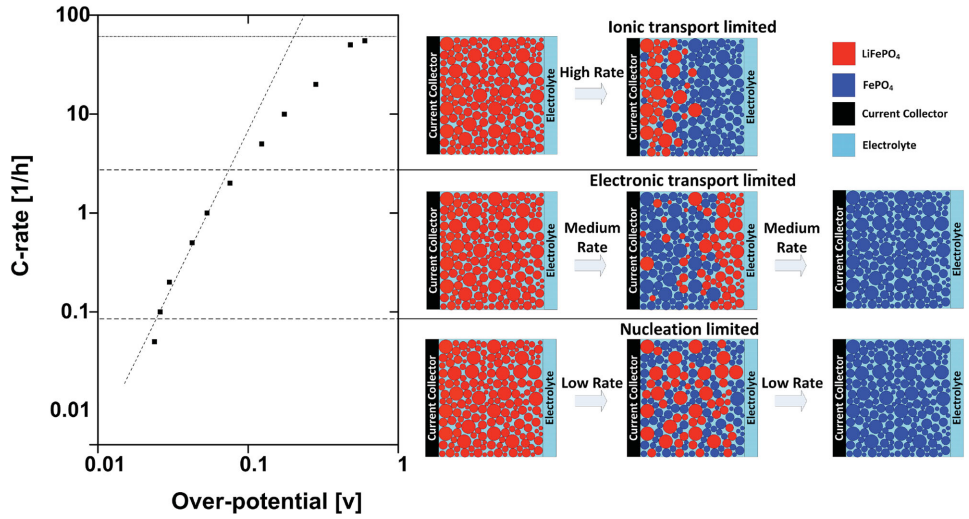

Figure 6. C-rate versus overpotential including a schematic representation of the observed Li-ion concentration profiles that allow to distinguish the different rate-limiting rate processes in the different rate regimes.

lower nucleation barriers as compared to larger particles. This reveals that nucleation barriers dominate the resistance against (dis)charging, consistent with extrapolation to a nonzero value of the overpotential at zero current density. At intermediate rates the relation between the current and overpotential is approximately linear, consistent with an Ohmic relation (for a linear plot see Figure S6 in the Supporting Information). This is in line with the observed depletion near the current collector upon charge, see Figures 4a and 5a, suggesting electronic conduction limitations at cycling rates between C/10 and 1 C. Finally, increasing the charge rate above 5 C leads to a larger increase in overpotential reflecting diffusion limited conditions consistent with the observed Li-ion depletion at the electrolyte side of the electrode upon charge shown in Figure 5c.

3. Conclusion

Using novel operando NDP measurements, the present results demonstrate that the rate-limiting charge transport phenomena in Li-ion battery electrodes depend not only on the electrode morphology and formulation, as should be expected, but also on the (dis)charge rate. This implies that depending on the applied (dis)charge a different route should be chosen to lower the internal resistance, and hence improve rate capacities and overall efficiency of Li-ion batteries. Thereby, in situ neutron depth profiling provides unique insight into the charge transport mechanism of Li-ion battery electrodes under realistic in operando conditions, a prerequisite for the improvement of Li-ion battery performance.

4. Experimental Section

Electrode Preparation: The cathode material was carbon-coated $LiFePO_4$ from Phostech with an average particle size of 140 nm. $LiFePO_4$ cathodes were prepared through mixing a slurry of $LiFePO_4$, Carbon Black (Super P), PVDF (polyvinylidene fluoride, Solvay), with a mass ratio of 80:10:10 respectively, in *N*-methylpyrrolidone (NMP). The carbon-rich sample was made with a mass ratio of the active material, carbon black (SuperP) and binder (PVDF) of 50:40:10. The slurries were spin coated on approximately 11.5 μm aluminum foil substrates. The bilayered electrodes of 140 nm $LiFePO_4$ particles and 70 nm $LiFePO_4$ particles were prepared using electrospraying. In this technique, a liquid electrode slurry flows from a capillary nozzle is dispersed into fine droplets by means of a high electric potential.[61,62] By controlling the voltage the rate of deposition can be manipulated and thus the thickness of the coating. Further details can be found in the Supporting Information. Glass fiber disks (Whatman) were used as separators and the electrolyte used was 1.0 molar $LiPF_6$ in EC/DMC (ethylene carbonate and dimethyl carbonate in a 1:1 ratio, Novolyte, battery grade). All the electrodes were pressed before use to ensure a good contact between active material and current collector. The battery components were assembled under argon atmosphere (<0.1 ppm O_2/H_2O) in a specially designed air-tight cell in which the current collector serves as window for the NDP experiments. All electrochemical tests were performed galvanostatically within a voltage window of 4.3 and 2.5 V versus Li/Li^+ using a Maccor 4000 or 4400 cycling system.

Neutron Depth Profiling: Neutron depth profiling was performed on one of the thermal neutron beam lines at the Reactor Institute Delft, The Netherlands. The NDP cell was positioned inside the vacuum chamber at an angle of 30° toward the incident neutron beam and parallel to the detector. For the current collector used (10.5 μm Al foil) the stopping power was too large for the ^4He particles to leave the battery. As such, only the energy loss of the ^3H particles was measured with the charged particle implanted Si detector. The energy spectrum was then collected by a multi channel analyzer (MCA). Figure 1 shows the schematic of the in situ NDP measurement setup. The depth calibration, relating the measured ^3H energy to the Li-ion depth position, was performed using SRIM and is further discribed in the Supporting Information.[63]

Supporting Information

Supporting Information is available from the Wiley Online Library or from the author.

Acknowledgements

The authors thank Daniel Cogswell for the stimulating discussions. The research leading to these results has received funding from the European Research Council under the European Union's Seventh Framework

Programme (FP/2007-2013)/ERC Grant Agreement no. [307161] of M.W. The authors would like to thank the Chinese Scholarship Council (CSC) for financially supporting part of the work in this paper. Financial support from the Advanced Dutch Energy Materials (ADEM) program of the Dutch Ministry of Economic Affairs, Agriculture and Innovation is gratefully acknowledged.

Received: March 11, 2015
Revised: May 7, 2015
Published online: June 10, 2015

[1] J. Newman, W. Tiedemann, *AIChE J.* **1975**, *21*, 25.
[2] M. Z. Bazant, *Acc. Chem. Res.* **2013**, *46*, 1144.
[3] A. K. Padhi, K. S. Nanjundaswamy, J. B. Goodenough, *J. Electrochem. Soc.* **1997**, *144*, 1188.
[4] N. E. A. Ravet, in *Electrochemical Society Fall Meeting, Electrochemical Society*, Pennington, NJ **1999**, 127.
[5] H. Huang, S. C. Yin, L. F. Nazar, *Electrochem. Solid State Lett.* **2001**, *4*, A170.
[6] P. S. Herle, B. Ellis, N. Coombs, L. F. Nazar, *Nat. Mater.* **2004**, *3*, 147.
[7] J. Maier, *Nat. Mater.* **2005**, *4*, 805.
[8] P. G. Bruce, B. Scrosati, J. M. Tarascon, *Angew. Chem. Int. Ed.* **2008**, *47*, 2930.
[9] A. S. Arico, P. Bruce, B. Scrosati, J. M. Tarascon, W. Van Schalkwijk, *Nat. Mater.* **2005**, *4*, 366.
[10] M. Wagemaker, F. M. Mulder, *Acc. Chem. Res.* **2013**, *46*, 1206.
[11] D. A. Cogswell, M. Z. Bazant, *Nano Lett.* **2013**, *13*, 3036.
[12] A. Van der Ven, M. Wagemaker, *Electrochem. Commun.* **2009**, *11*, 881.
[13] J. Maier, *Angew. Chem. Int. Ed.* **2013**, *52*, 4998.
[14] S. Ganapathy, M. Wagemaker, *ACS Nano* **2012**, *6*, 8702.
[15] N. Meethong, H. Y. S. Huang, W. C. Carter, Y. M. Chiang, *Electrochem. Solid State Lett.* **2007**, *10*, A134.
[16] K. T. Lee, W. H. Kan, L. F. Nazar, *J. Am. Chem. Soc.* **2009**, *131*, 6044.
[17] X. Zhang, M. van Hulzen, D. P. Singh, A. Brownrigg, J. P. Wright, N. H. van Dijk, M. Wagemaker, *Nano Lett.* **2014**, *14*, 2279.
[18] H. Liu, F. C. Strobridge, O. J. Borkiewicz, K. M. Wiaderek, K. W. Chapman, P. J. Chupas, C. P. Grey, *Science* **2014**, 344.
[19] P. Bai, D. A. Cogswell, M. Z. Bazant, *Nano Lett.* **2011**, *11*, 4890.
[20] D. A. Cogswell, M. Z. Bazant, *ACS Nano* **2012**, *6*, 2215.
[21] R. Malik, F. Zhou, G. Ceder, *Nat. Mater.* **2012**, *10*, 587.
[22] B. Kang, G. Ceder, *Nature* **2009**, *458*, 190.
[23] D. Y. W. Yu, K. Donoue, T. Inoue, M. Fujimoto, S. Fujitani, *J. Electrochem. Soc.* **2006**, *153*, A835.
[24] J. Jamnik, R. Dominko, B. Erjavec, M. Remskar, A. Pintar, M. Gaberscek, *Adv. Mater.* **2009**, *21*, 2715.
[25] C. Fongy, S. Jouanneau, D. Guyomard, J. C. Badot, B. Lestriez, *J. Electrochem. Soc.* **2010**, *157*, A1347.
[26] C. Fongy, A. C. Gaillot, S. Jouanneau, D. Guyomard, B. Lestriez, *J. Electrochem. Soc.* **2010**, *157*, A885.
[27] P. A. Johns, M. R. Roberts, Y. Wakizaka, J. H. Sanders, J. R. Owen, *Electrochem. Commun.* **2009**, *11*, 2089.
[28] J. Zhou, D. Danilov, P. H. L. Notten, *Chem. Eur. J.* **2006**, *12*, 7125.
[29] M. Gaberscek, J. Jamnik, *Solid State Ionics* **2006**, *177*, 2647.
[30] D. P. Singh, F. M. Mulder, A. M. Abdelkader, M. Wagemaker, *Adv. Energy Mater.* **2013**, *3*, 572.
[31] V. Srinivasan, J. Newman, *J. Electrochem. Soc.* **2004**, *151*, A1517.
[32] M. Safari, C. Delacourt, *J. Electrochem. Soc.* **2011**, *158*, A63.
[33] G. K. Singh, G. Ceder, M. Z. Bazant, *Electrochim. Acta* **2008**, *53*, 7599.
[34] T. R. Ferguson, M. Z. Bazant, *J. Electrochem. Soc.* **2012**, *159*, A1967.
[35] M. E. Holtz, Y. Yu, D. Gunceler, J. Gao, R. Sundararaman, K. A. Schwarz, T. A. Arias, H. D. Abruna, D. A. Muller, *Nano Lett.* **2014**, *14*, 1453.
[36] K. A. See, M. Leskes, J. M. Griffin, S. Britto, P. D. Matthews, A. Emly, A. Van der Ven, D. S. Wright, A. J. Morris, C. P. Grey, R. Seshadri, *J. Am. Chem. Soc.* **2014**, *136*, 16368.
[37] K. Ogata, E. Salager, C. J. Kerr, A. E. Fraser, C. Ducati, A. J. Morris, S. Hofmann, C. P. Grey, *Nat. Commun.* **2014**, *5*.
[38] J. B. Siegel, X. Lin, A. G. Stefanopoulou, D. S. Hussey, D. L. Jacobson, D. Gorsich, *J. Electrochem. Soc.* **2011**, *158*, A523.
[39] L. G. Butler, B. Schillinger, K. Ham, T. A. Dobbins, P. Liu, J. J. Vajo, *Nucl. Instrum. Methods Phys. Res. A* **2011**, *651*, 320.
[40] G. V. Riley, D. S. Hussey, D. L. Jacobson, *ECS Trans.* **2010**, *25*, 75.
[41] J. Wang, D. X. Liu, M. Canova, R. G. Downing, L. R. Cao, A. C. Co, *J. Radioanal. Nucl. Chem.* **2014**, *301*, 277.
[42] J. F. M. Oudenhoven, F. Labohm, M. Mulder, R. A. H. Niessen, F. M. Mulder, P. H. L. Notten, *Adv. Mater.* **2012**, *23*, 4103.
[43] X. Zhang, M. Wagemaker, IMLB 2014 poster abstract, https://ecs.confex.com/ecs/imlb2014/webprogram/Paper35552.html (accessed: May 2015).
[44] M. Wagemaker, Abstract Mon-A1-07 Solid State Ionics 19 Kyoto, 2013 (accessed: June 2015).
[45] M. Wagemaker, Abstract SSE 2013, http://sse2013.uni-hd.de/Abstracts/abstract_Wagemaker_SSE2013.pdf (accessed: June 2015).
[46] D. X. Liu, J. Wang, K. Pan, J. Qiu, M. Canova, L. R. Cao, A. C. Co, *Angew. Chem.Int. Ed.* **2014**, *53*, 9498.
[47] J. F. Ziegler, G. W. Cole, J. E. E. Baglin, *J. Appl. Phys.* **1972**, *43*, 3809.
[48] R. G. Downing, R. F. Fleming, J. K. Langland, D. H. Vincent, *Nucl. Instrum. Methods* **1983**, *218*, 47.
[49] J. P. Biersack, D. Fink, R. Henkelmann, K. Muller, *Nucl. Instrum. Methods* **1978**, *149*, 93.
[50] S. S. R. B. Whitney, Y. H. Huang, J. B. Goodenough, *J. Electrochem. Soc.* **2009**, *156*, A886.
[51] S. C. Nagpure, P. Mulligan, M. Canova, L. R. Cao, *J. Powder Sources* **2014**, *248*, 489.
[52] S. C. Nagpure, R. G. Downing, B. Bhushan, S. S. Babu, L. Cao, *Electrochim. Acta* **2011**, *56*, 4735.
[53] S. C. Nagpure, R. G. Downing, B. Bhushan, *Scr. Mater.* **2012**, *67*, 669.
[54] J. F. M. Oudenhoven, F. Labohm, M. Mulder, R. A. H. Niessen, F. M. Mulder, P. H. L. Notten, *Adv. Mater.* **2011**, *23*, 4103.
[55] T. R. Ferguson, M. Z. Bazant, *Electrochim. Acta* **2014**, *146*, 89.
[56] J. Maier, *Solid State Ionics* **2002**, *154*, 291.
[57] K. West, T. Jacobsen, S. Atlung, *J. Electrochem. Soc.* **1982**, *129*, 1480.
[58] M. Doyle, J. Newman, *J. Appl. Electrochem.* **1997**, *27*, 846.
[59] M. Thunman, K. Marquardt, R. Hahn, D. Kober, O. Goerke, H. Schubert, *ECS Trans.* **2012**, *41*, 147.
[60] V. Srinivasan, J. Newman, *Electrochem. Solid State Lett.* **2006**, *9*, A110.
[61] G.-T. Esteban, *Advanced Thin Layer Deposition of Materials for Li-Ion Batteries via Electrospray*, Delft University of Technology, Delft, The Netherlands **2014**.
[62] J. Grace, J. Marijnissen, *J. Aerosol Sci.* **1994**, *25*, 1005.
[63] J. F. Ziegler, M. D. Ziegler, J. P. Biersack, *Nucl. Instrum. Methods B* **2010**, *268*, 1818.